Alma Mater Studiorum Università di Bologna
Archivio istituzionale della ricerca

Coupled Electronic and Nuclear Motions during Azobenzene Photoisomerization Monitored by Ultrafast Electron Diffraction

(Article begins on next page)

Coupled electronic and nuclear motions during azobenzene photoisomerization monitored by ultrafast electron diffraction

Jérémy R. Rouxel,[*,†,‡] Daniel Keefer,[*,†] Flavia Aleotti,[¶] Artur Nenov,[¶] Marco Garavelli,[¶] and Shaul Mukamel[*,†]

†Department of Chemistry and Physics & Astronomy, University of California, Irvine, California 92697-2025, USA.

‡Univ Lyon, UJM-Saint-Etienne, CNRS, Graduate School Optics Institute, Laboratoire Hubert Curien UMR 5516, Saint-Etienne F-42023, France.

¶Dipartimento di Chimica Industriale, Università degli Studi di Bologna, Viale del Risorgimento 4, I-40136 Bologna, Italy.

E-mail: jeremy.rouxel@univ-st-etienne.fr; dkeefer@uci.edu; smukamel@uci.edu

Abstract

Ultrafast electron diffraction is a powerful technique that can resolve molecular structures with femtosecond and angstrom resolutions. We demonstrate theoretically how it can be used to monitor conical intersection dynamics in molecules. Specific contributions to the signal, which vanish in the absence of vibronic coherence and offer a direct window into conical intersection paths, are identified. A special focus is on hybrid scattering from nuclei and electrons, a process that is unique to electron (rather than X-ray) diffraction and monitors the strongly coupled nuclear and electronic motions in the vicinity of conical intersections. An application is made to the cis to trans

1

isomerization of azobenzene, computed with exact quantum dynamics wavepacket propagation in a reactive two-dimensional nuclear space.

1 Introduction

Ultrafast Electron Diffraction (UED) is a well established technique that can resolve in space and time molecular structures as they undergo ultrafast dynamics.[1,2] It can potentially be more sensitive than time-resolved X-ray Diffraction (XRD) due to the stronger interaction between electrons and molecules compared to photons.[3] Space charge effects have limited the atomic and temporal resolution required to follow ultrafast femtosecond dynamics.[4,5] Additionally, low signal-to-noise ratios also limit the ability to deconvolve the signal and the instrument response function, which is crucial for a high temporal resolution.[5,6] An important effort has been recently directed at improving the resolution of electron pulse sources using nonrelativistic[7] or relativistic[6] sources. Recent experiments are pushing the temporal limits of observable dynamical pathways to the femtosecond regime.[8–11]

Most UED studies have so far focused on resolving the evolving structure of electronically excited molecules undergoing photophysical and photochemical processes.[12] These have led to striking observations of electronic and nuclear relaxation. However, time-resolved diffraction signals are not solely determined by the time dependent charge density but should be dissected into various contributions, each having a distinct physical significance.[13,14] The UED diffraction pattern originates from both the electronic σ_E and the nuclear σ_N molecular charge densities. The UED signal from a single molecule is given by a two-point correlation function of the total (electronic + nuclear) charge density. As such, it contains purely electronic, purely nuclear and hybrid electronic and nuclear contributions. The purely electronic terms are the same as in XRD,[15,16] up to a prefactor, and this component of UED signals thus carries the same information as XRD. When

this contribution is further expanded in molecular eigenstates, it is possible to single out terms sensitive to molecular coherences.[13,17] The nuclear and hybrid terms, which do not appear in XRD, offer novel insights into the molecular dynamics and are highly sensitive to conical intersections (CoIns).

Azobenzene has two stable trans and cis isomers in the electronic ground state, see Fig 1. Its photoisomerization has drawn considerable interest for photoswitching application in materials,[18] neurons[19] and protein folding.[?] Selective optical switching between the two isomers with high quantum yield is possible by using different wavelengths. The isomerization is triggered by photoexcitation from the S_0 to the $n\pi^*$ S_1 state.[20,21] High-level CASPT2 potential energy surfaces in the reduced space of three nuclear degrees of freedom describing the isomerization reaction were reported in.[22] The first nuclear coordinate is the Carbon-Nitrogen-Nitrogen-Carbon (CNNC) dihedral angle connecting the cis minimum at $5°$ with the trans minimum at $180°$. The second and third coordinate are the two respective CNN bending angles between the two Nitrogen atoms and one adjacent Carbon atom, respectively. To simulate nuclear wavepacket dynamics for the cis to trans isomerization, it is sufficient to include one of the two CNN angles, while the other one remains fixed at $116°$.[13] Symmetry breaking between both angles is necessary to reach the minimum energy conical intersection, that spans a strong non-adiabatic coupling seam between CNN=$127°$ and $152°$. Hybrid pathways have been discussed and known as rotation-assisted inversion or inversion-assisted rotation. The isomerization dynamics timescale exhibits a multi-exponential decay with timescales ranging from $\approx$ 0.2 ps to $\approx$ 12 ps[23] for the dynamics in the S_1 state. In Fig.2, the nuclear wavepacket amplitude squared is displayed as a function of the torsion and bending angles for different times delays (0, 100 and 200 fs). The average molecular geometry is displayed for each of these three times.

In section 2, we first summarize how the UED signal can be dissected into multiple interaction pathways. Next, we present how the various contributions to the signal, i.e.

3

elastic/inelastic and electronic/nuclear contributions, offer different windows into the ultrafast isomerization dynamics. In section 3, we discuss how these contributions can be discriminated experimentally.
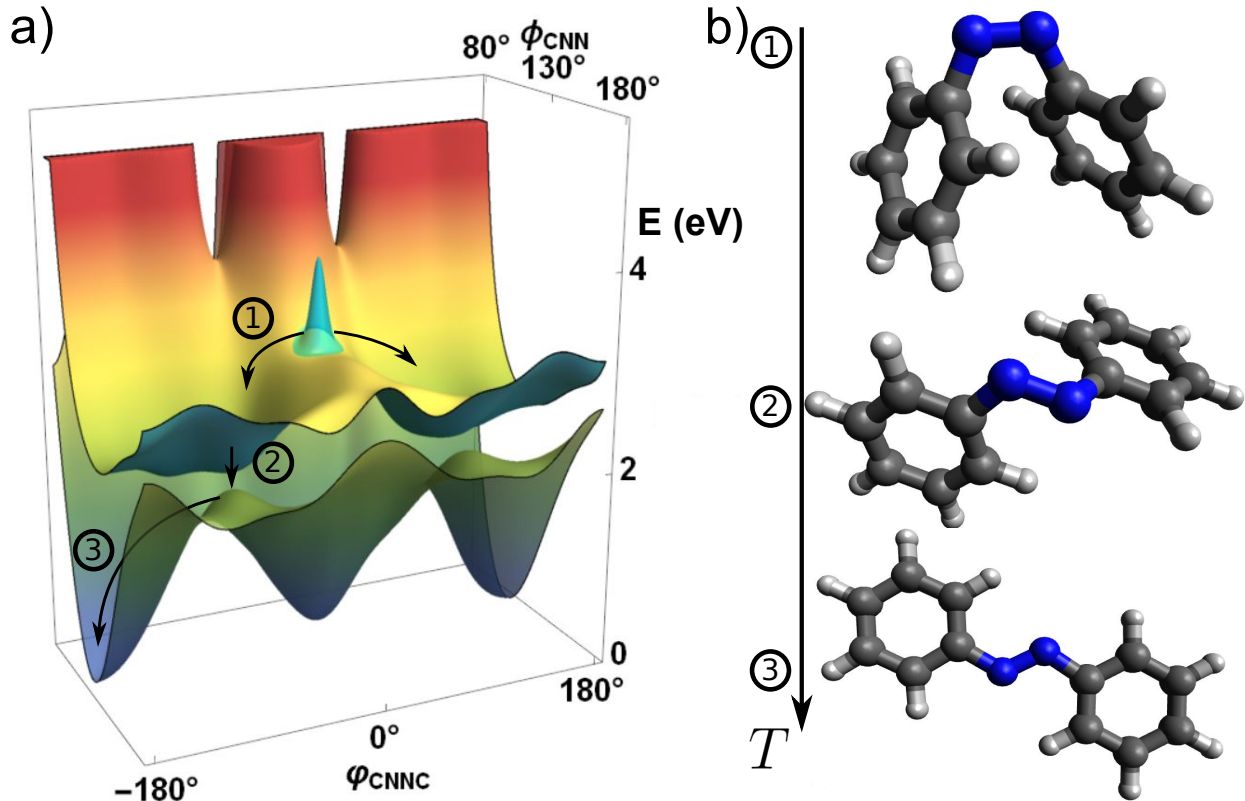
Figure 1: a) The S_0 and S_1 potential energy surfaces of azobenzene. The wavepacket in 1 is initially localized around the cis geometry in the S_1 state and moves toward the CoIn in 2. After crossing the CoIn, the wavepacket reaches the trans geometry within few hundreds femtoseconds. b) Single point geometries of the cis (1), trans (3) isomers and at the CoIn (2).

2 Results

The UED signals

The UED signal is defined in appendix and is given by:[14]

$$S_{\text{UED}}(\boldsymbol{q}, T) = \frac{2}{\epsilon_0^2 \hbar^2} \frac{1}{q^4} \Re \int dt dt' \langle \sigma_T(-\boldsymbol{q}, t) \sigma_T(\boldsymbol{q}, t') \rangle F_e(t) F_e^*(t') e^{i\omega_s(t-t')} \tag{1}$$

4
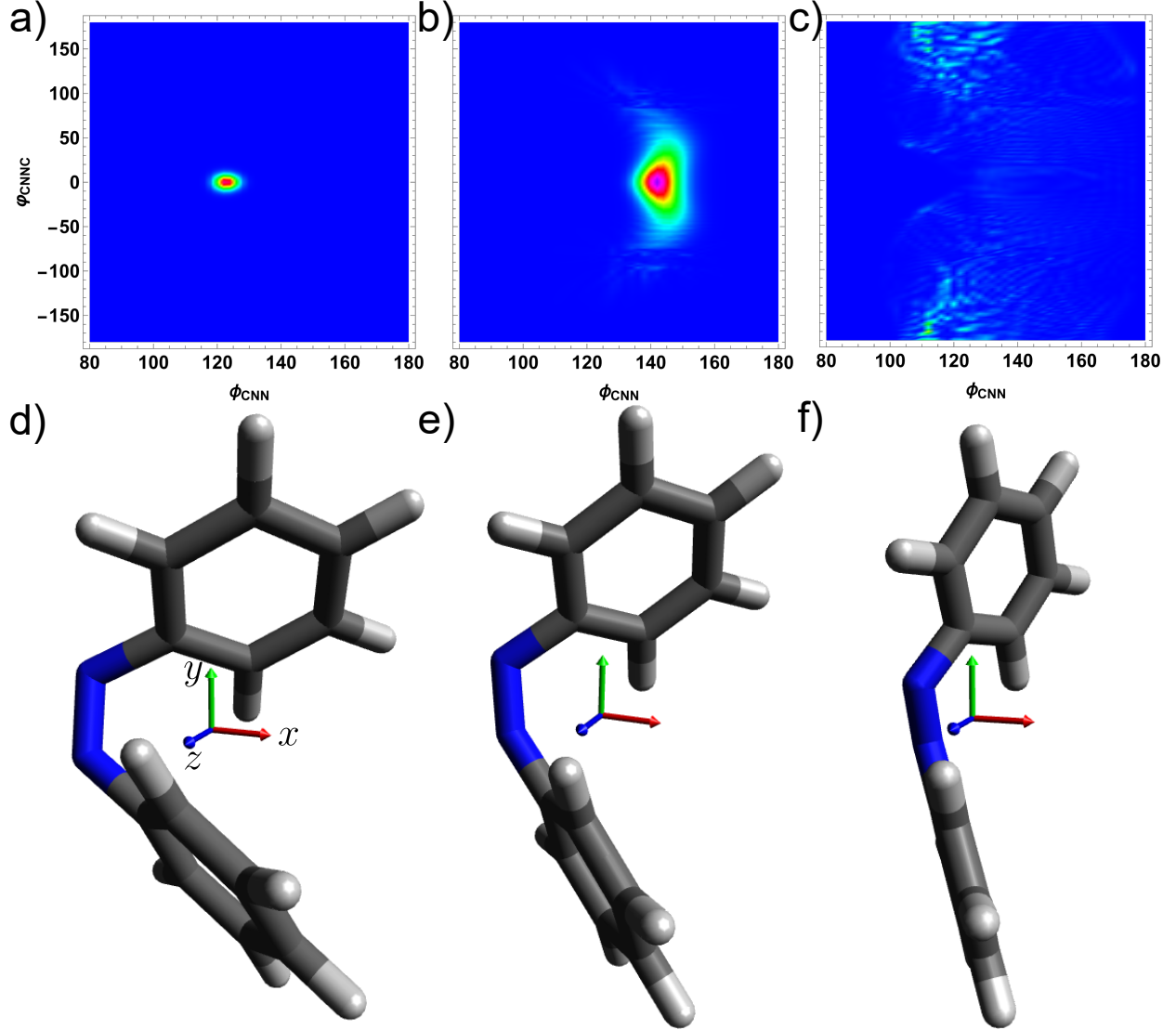
Figure 2: Amplitude squared of the excited state wavepacket at $T = 0$, 100 and 200 fs in panels a), b) and c) respectively. Panels d), e) and f) show the corresponding averaged molecular geometries at the same time delays.

where $\boldsymbol{q} = \boldsymbol{k}_s - \boldsymbol{k}_e$ is the momemtum transfer between the scattered and incoming electron beams with wavevectors $\boldsymbol{k}_s$ and $\boldsymbol{k}_e$ respectively. $\sigma_T = \sigma_E + \sigma_N$ is the total charge density given by the sum of the unscreened electronic σ_E and nuclear σ_N charge densities. F_e is the electron beam temporal envelope. Eq. 1 can be further simplified by assuming that 1) no field is initially present in the detector direction (homodyne detection), 2) the signal originates from a single molecule, 3) the electron pulse is impulsive $F(t) = \delta(t - T)$.

5

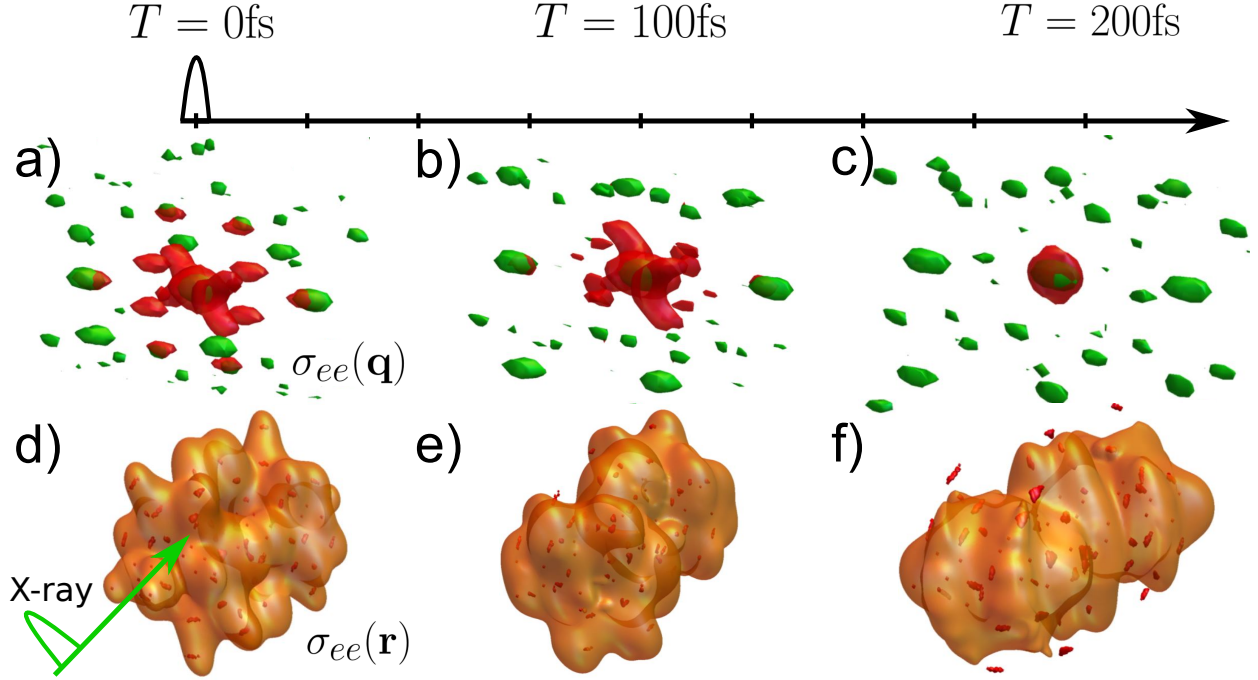Figure 3: Charge densities at 0, 100 and 200 fs after the actinic excitation. Panels a), b) and c) display the Fourier transform of the charge densities measured in a UED experiment. The electronic and nuclear contribution are in red and green respectively. Corresponding real space electronic (orange) and nuclear (red) charge densities of the e state are shown in panels d), e) and f).

Under these conditions, Eq. 1 becomes:

$$S_{\text{UED}}(\boldsymbol{q}, T) \propto \frac{1}{q^4} \langle \Psi(T) | \sigma_T(-\boldsymbol{q}) \sigma_T(\boldsymbol{q}) | \Psi(T) \rangle \tag{2}$$

The electrons+nuclei wavefunction $|\Psi(T)\rangle = \sum_i |\chi_i(T)\rangle |\varphi_i\rangle$ is expanded in the adiabatic basis set consisting of products of nuclear $|\chi_i(T)\rangle$ and electronic $|\varphi_i\rangle$ many-body states in state i. T is the delay between the initial actinic pulse launching the dynamics and the electron beam scattering event.

These expressions have close similarities with the tr-XRD signal[13] but with some notable differences: XRD only involves the electronic charge density while UED depends on the total electronic+nuclear charge density. In addition, the $1/q^4$ prefactor dampens the high q contributions. By expanding the two-point correlation function in Eq. 2 in the

valence electronic states, the 12 contributions to the UED signal can be expressed by the loop diagrams, given in Fig. 8 in the materials and methods section.

$$S_{\text{UED}}(\boldsymbol{q}, T) \propto \sum_{i=1}^{12} S_{\text{UED}}^{\text{D}i}(\boldsymbol{q}, T) \tag{3}$$

Application to the cis-trans isomerization of azobenzene

All 12 contributions to the UED signal[14] were calculated for oriented azobenzene molecules. The fixed laboratory frame is displayed in panels d), e) and f) of Fig. 2. The potential energy surfaces (PES) of the S_0 and the S_1 states, see Fig. 1 were computed by ab initio quantum chemistry using RASSCF and RASPT2 modules with MOLCAS8.[24] The wavepacket propagation was simulated by solving the time-dependent Schrödinger equation numerically in the reduced two-dimensional space spanned by the CNN bond angle and the the CNNC dihedral angle. Details are given in the methods section. Charge density matrix elements in the electronic space were computed on a numerical grid for the nuclear coordinates, and their products were averaged over the nuclear wavepacket to obtain the necessary charge density matrix elements for single molecule signals. Diagonal and off-diagonal matrix elements of the charge density operator averaged over the nuclear wavepacket are displayed in Fig. 3.

The simulated UED signal, Eq. 3, is depicted in Fig. 4. To eliminate the divergence at the origin, the signal has been multiplied by q^4. At $T = 0$ fs, the excited nuclear wavepacket located in the S_1 state is represented by a Gaussian wavepacket centered at the cis geometry. It reaches the CoIns after 70fs at the geometry (2) displayed in Fig. 1. This assumes an excitation of 100% of the ground state into the S_1 state.[25] Experimental excitations are usually lower to keep the process in the linear regime and avoid multi-photon processes. A lower than 100% excitation adds a constant background from elastic ground state scattering to the signal. This only affects the relative strengths of the different signatures, but not the qualitative features. Scattering experiments and analysis with

7
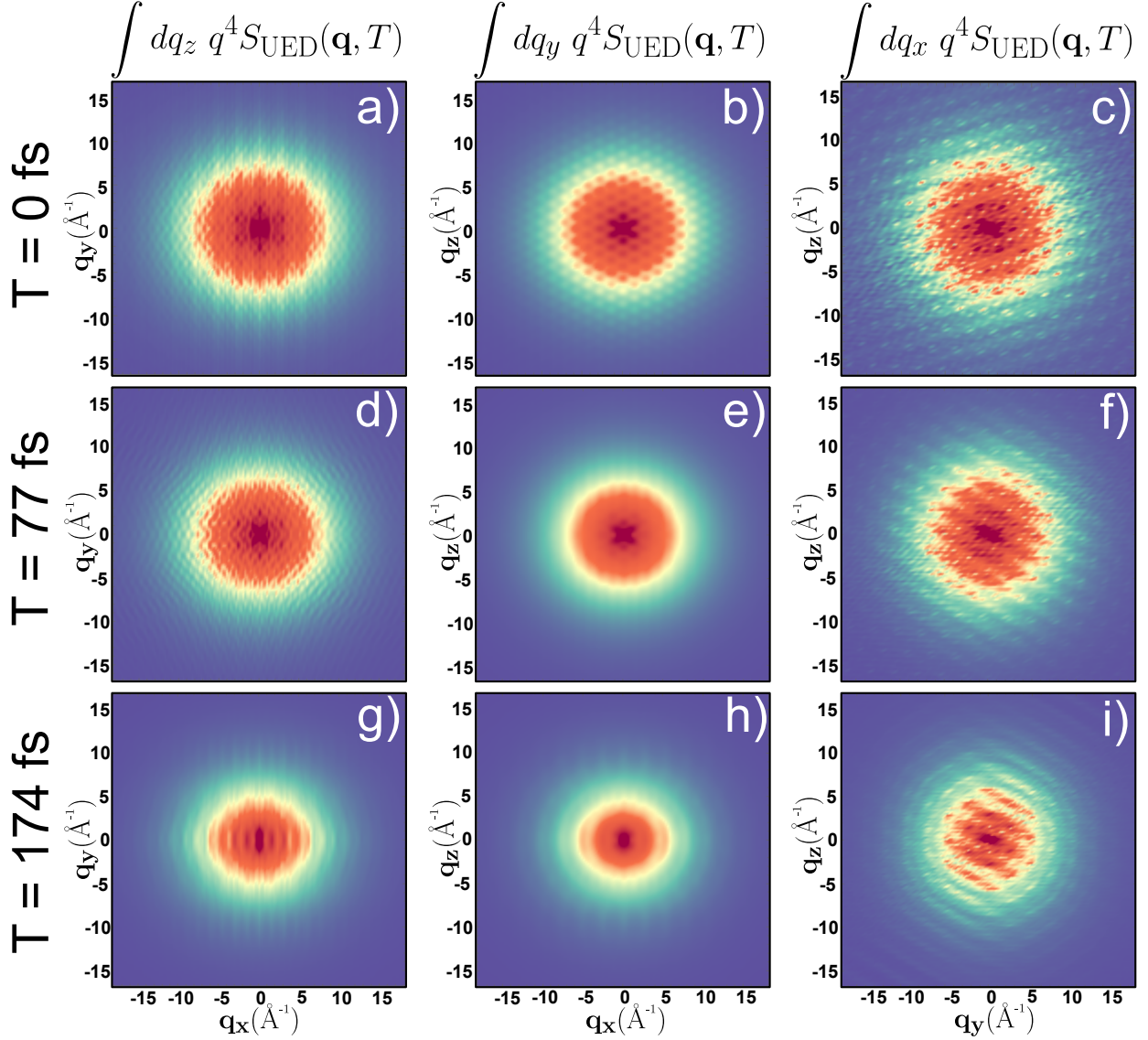
Figure 4: UED diffraction patterns at the initial time (top), at 80 fs when the CoIn is reached (middle) and at 170 fs (bottom) and for different projections in q space along q_z (panels a, d, g), q_y (panels b, e, h) and q_x (panels c, f, i).

low excitation ratios (around 5%) have been demonstrated.[26]

Fig. 5 displays the electronic, nuclear and hybrid contributions to the UED signal in $q - T$ space along the q_x, q_y or q_z. The top row shows the total signal. The electronic contribution, diagrams 1 to 6 in Fig. 8 (materials and methods), displayed in the second row, is the main contribution to the total signal and has already been studied previously for tr-XRD.[13] A careful inspection shows some minor differences between the total sig-
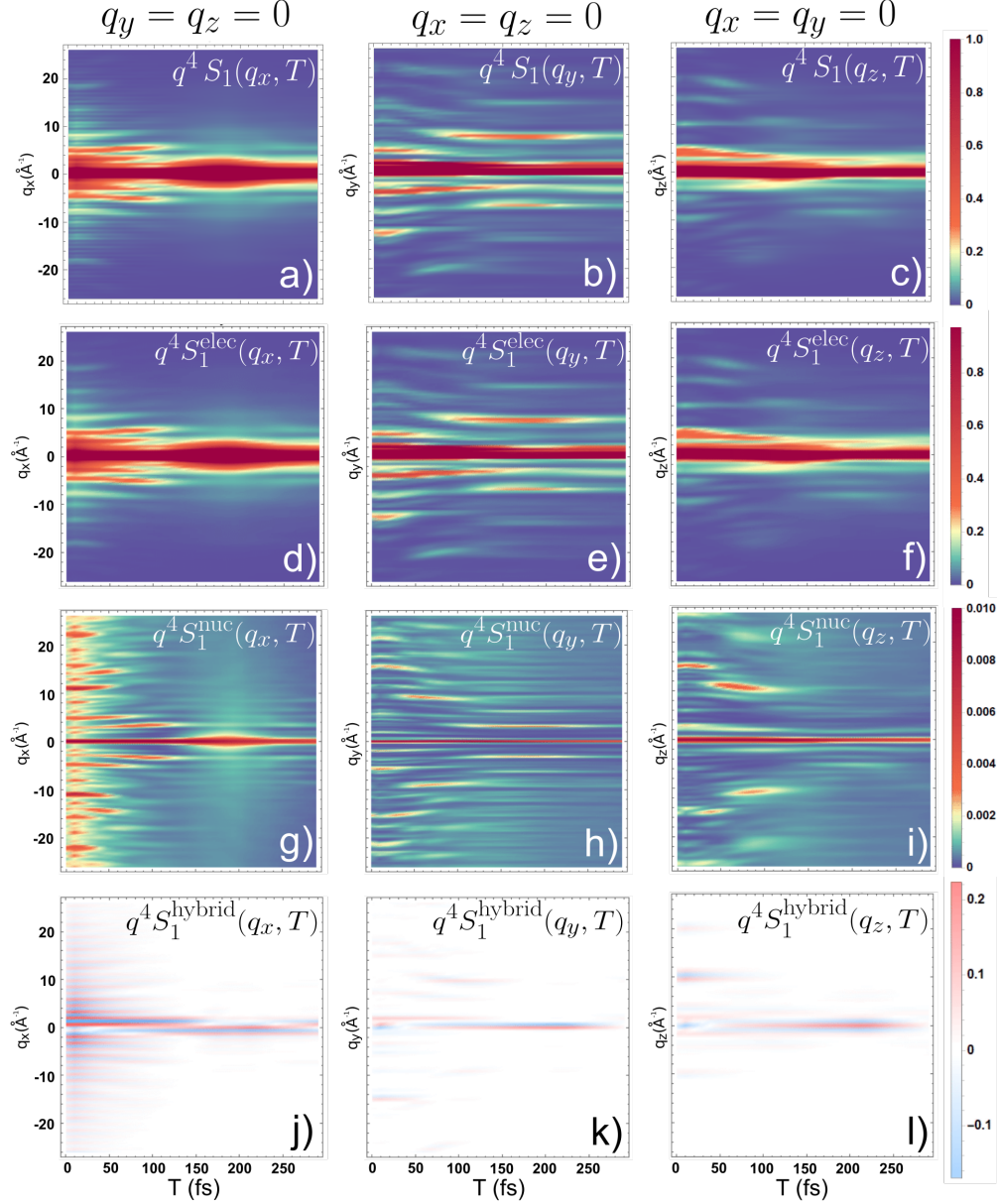
Figure 5: Total (panels a), b) and c)), electronic (panels d), e) and f)), nuclear (panels g), h) and i)) and hybrid (panels j), k) and l)) contributions to UED along q_x, q_y and q_z from left to right. The electronic contribution is the sum of diagrams (i) to (vi of Fig. 8) of the UED. The nuclear contribution is the sum of diagrams (vii) and (viii) and the hybrid electronic/nuclear contribution is the sum of diagrams (ix) to (xii).

nal and the electronic contribution, especially at short time and large q values where the nuclei contributions are visible. This signal displays a particular sensitivity to the CoIn. Along q_y for example, the signal at $q_y = 5$ Å^{-1} starts fading at $T = 70$ fs when the CoIn is being crossed while another feature appears at $q_y = 8$Å^{-1}. The 2nd row shows the

9

nuclear contributions to the signal, given by diagrams 7 and 8 in Fig. 8 (materials and methods). Initially, the nuclear wavepacket is well localized at the cis geometry and the atomic nuclear charges are centered around their atomic sites. This is why the nuclear signal is more delocalized in q space than its electronic counterpart at the beginning of the dynamics. As the nuclear wavepacket spreads, the electronic density at the atomic sites becomes more delocalized and the signals are dominated by the lower q values as shown in Fig. 5. The nuclear contribution contains features at multiple q values that vanish when the CoIn is reached. Finally, the hybrid electronic/nuclear terms are displayed at the bottom row of Fig.5. These are mostly located around low q values where both the electronic and nuclear charge densities overlap in q space. Along q_y, the signal contains a clear feature at 10Å^{-1} that appears at the onset of the CoIn at 70 fs and vanishes at 170 fs with the vanishing of the coherence between the S_0 and the S_1 state (Fig. 3b). While the electronic contributions in the top row are observable with X-ray diffraction as well, the nuclear and hybrid terms in the middle and bottom rows are unique to UED.

A different partitioning of the 12 contributions to the signal is presented in Fig. 6. The top row depicts the elastic contributions (diagrams D1, D2, D7, D8, D9, D10, see Fig. 8) whereas the bottom row displays the inelastic contributions to the signal (D3, D4, D5, D6, D11, D12). The inelastic signal reveals the most direct information on the CoIn since it is induced by the coherence created as the CoIn is being crossed.

3 Discussion

Each diagram contributing to the UED signals carries a distinct information regarding the molecular dynamics. The electronic (second row, Fig. 5) and nuclear (third row, Fig. 5) contributions to the signal measure Fourier transforms of the two-point correlation functions of the electronic and nuclear charge densities respectively. Additionally, the hybrid electronic/nuclear terms (bottom row, Fig. 5) possess unique features of the CoIns
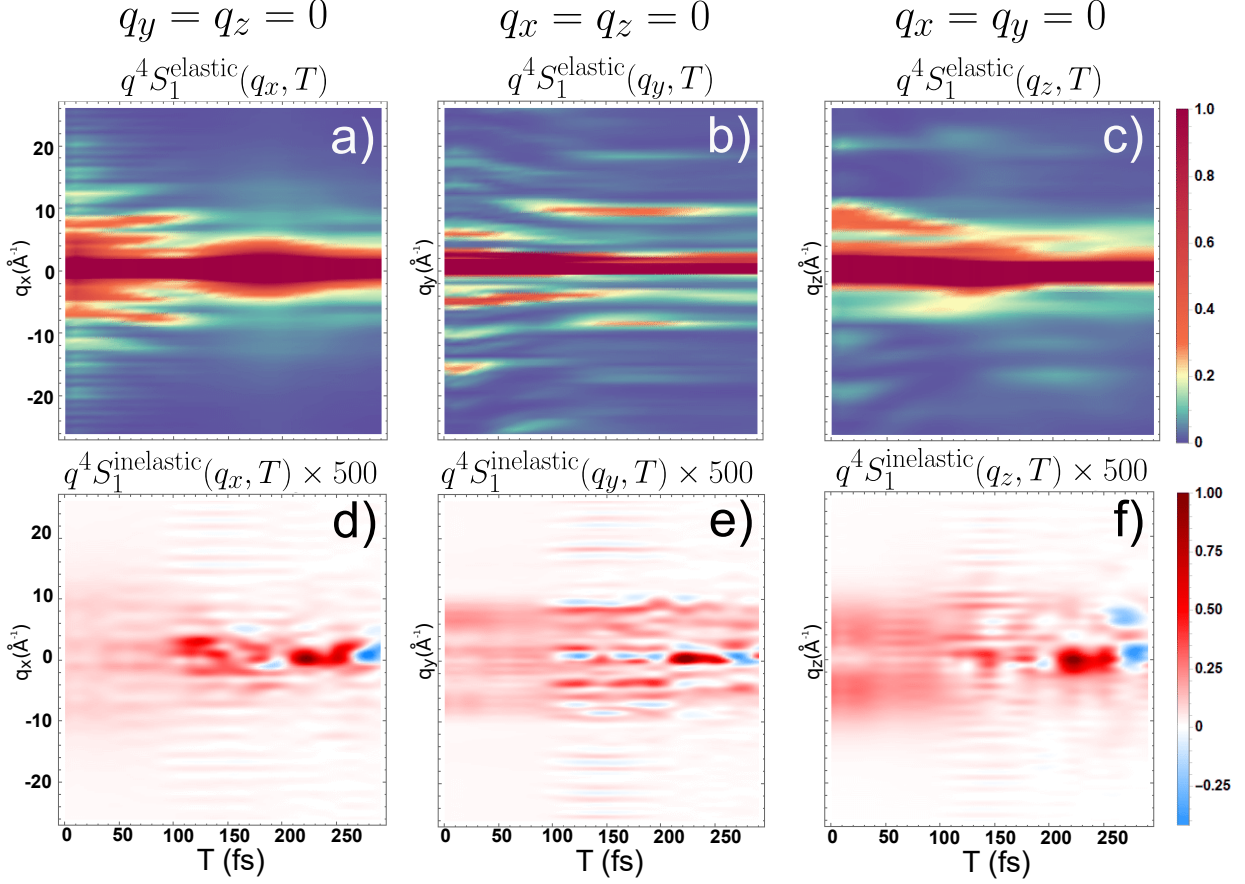
Figure 6: Elastic(panels a, b, c) and inelastic (panels d, e, f) contributions to UED. Top: Sum of the elastic contributions (diagrams (i), (ii), (vii), (viii), (ix) and (x)). Bottom: Sum of the inelastic contributions (diagrams (iii), (iv), (v), (vi), (xi) and (xii)).

region. The hybrid contributions to UED in the q-values above 5 Å^{-1}, zoomed in Fig. 7b, are very sensitive to the passage through the CoIn as can be compared with the dynamics of the coherence showed in Fig. 7a. The ability to extract them from the total signal would be an invaluable tool to study the dynamics. At conical intersections, the electrons and nuclei move on a comparable timescale and thus become strongly coupled. The hybrid nuclear/electronic term, that is unique to UED, is the most adequate one to observe this coupled motion.

The elastic terms contain products of diagonal matrix elements of the charge density operator that scale as the square of the number of electrons N^2 in the molecule. On the other hand, the inelastic terms have the scaling of a single valence electron and are there-

fore much weaker. Nonetheless, they can be separated by energy resolved detection since the scattered electron is shifted in energy by few electron-volts. Finally, by subtracting the different contributions to the frequency-resolved signal from the one without frequency resolution, one can recover the hybrid terms.

Since the electronic charge density is more delocalized than the nuclear one, its contribution to the diffraction pattern is limited to smaller momentum transfer values. At high q the signal is thus dominated by the nuclear terms. Separating the contributions at smaller q, up to few Å^{-1} is a more delicate task which will require to use information derived from other measurements.[27] The XRD diffraction pattern is produced by the electronic charge density. Similarly, neutron diffraction patterns solely originate from the nuclear charge density. By proper scaling, e.g. following the Mott-Bethe formula for XRD,[28] one can subtract these contributions from the UED signal to single out the hybrid electronic/nuclear terms. The UED signal can be alternatively analyzed in combination with time-resolved photoelectron spectroscopy (TRPES) to extract additional energy information.[29]

4 Conclusions

In this work, we have addressed the dissection of UED signals to extract additional information on the dynamics. A perturbative loop diagrams description reveals the existence hybrid electronic/nuclear terms present in the signal. Although these terms are weaker than their purely electronic or nuclear counterparts, they display a high sensitivity to the nuclear dynamics, especially at conical intersections. Experimental efforts targeted at extracting these hybrid contributions should be valuable to gain further insight into non-adiabatic dynamics.

To highlight the features of the proposed signal, we have considered an idealized configuration in which the molecule was perfectly oriented. Also, the dynamics in the

present study starts with a nuclear wavepacket fully in the excited state. A more realistic approach would assume an extra pump pulse and a partial population into the excited state. Future work should consider the case of full or partial rotational averaging and include explicitly the pump pulse in the propagation.

Finally, we demonstrated that UED is sensitive to both electronic and nuclear dynamics, not only to structural changes. This point was also made recently by de Kock et al.[30]
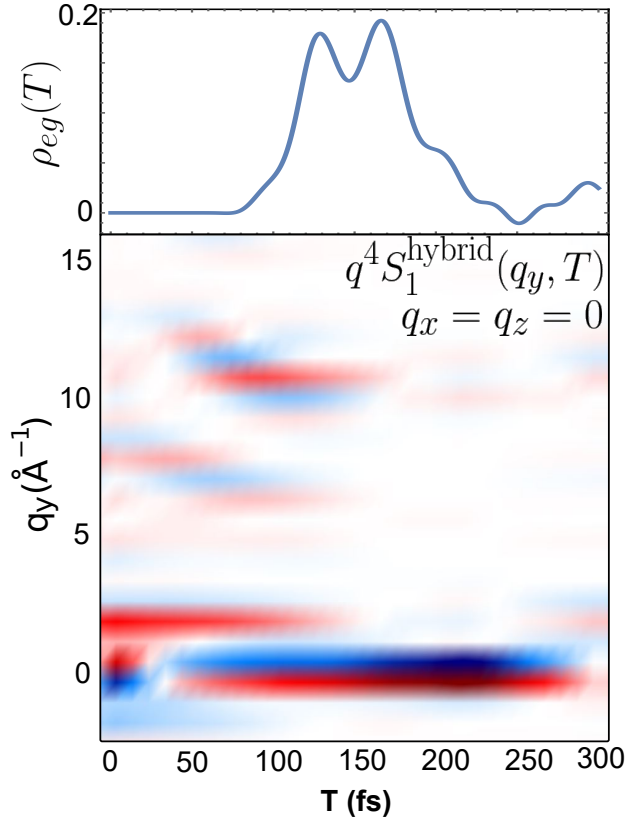

Figure 7: Top: Time evolution of the coherence $\rho_{eg}(T)$. Bottom: Zoom on the hybrid contribution to the signal. The feature at 10Å^{-1} appears at 70 fs and disappears at 170 fs, matching with the lifetime of the coherence created at the CoIn.

Materials and methods

Signal definitions

The molecule-beam interaction Hamiltonian for ultrafast ED is

$$H_{\text{int}}^{\text{UED}} = \int d\boldsymbol{r} d\boldsymbol{r}' \, \frac{\sigma_T(r)\sigma_B(r')}{4\pi\epsilon_0|\boldsymbol{r} - \boldsymbol{r}'|} \tag{4}$$

where $\sigma_T(\boldsymbol{r}) = \sigma_E(\boldsymbol{r}) + \sigma_N(\boldsymbol{r})$ is the total molecular charge density operator (electron + nuclei) and $\sigma_B(r')$ is the one of the incoming electron beam.

The UED signal is defined by the integrated rate of change of the electron number $\langle \dot{N}_{k_e} \rangle$ in the detector direction:

$$S_{\text{UED}}(\boldsymbol{k}_e) = \int dt \langle \dot{N}_{k_e} \rangle \tag{5}$$

where $\boldsymbol{k}_e$ is the momentum of the observed electron. By pertubatively expanding the expectation value into the interaction Hamiltonian of the incoming electron beam, Eq.4, the expression of the UED signal, Eq. 1 is obtained.

Closed expressions of the UED signal can be obtained by summing over molecular eigenstates and by separating the charge densities into their electronic and nuclear origins. The resulting contributions are represented by the 12 diagrams depicted in Fig. 8.

Wavepacket Simulations

To model azobenzene photoisomerization, we perform exact nuclear wavepacket simulations according to the time–dependent Schrödinger equation

$$i\hbar \frac{\partial}{\partial t} \psi = \hat{H}\psi = \left[\hat{T}_q + \hat{V} \right] \psi \tag{6}$$
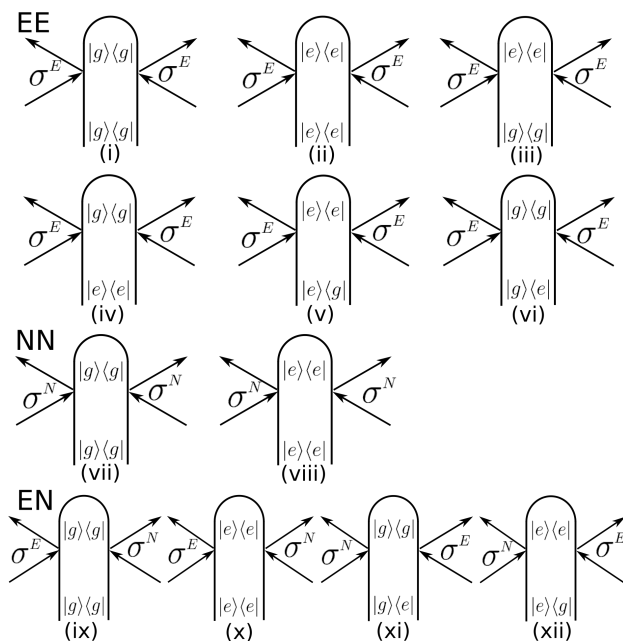
Figure 8: The loop diagrams representing the UED signal. The first two rows are purely electronic contributions also measured by tr-XRD. The third row corresponds to scattering off the nuclear part of the charge density. The bottom row represents the hybrid electronic/nuclear scattering.

in the reduced-dimensional space of two reactive coordinates q. In Eq. 6, ψ is the nuclear wavepacket, and $\hat{T}_q$ and $\hat{V}$ are the kinetic and potential energy operator. As identified in Refs.,[13,22] two nuclear coordinates are relevant for the *cis → trans* photoisomerization. The first one is the reactive Carbon–Nitrogen–Nitrogen–Carbon (CNNC) torsion that connects the *cis* and *trans* structures at $0°$ and $\pm180°$. The second coordinate is one of the two CNN bending angles between the *azo*–unit and one of the two benzene rings, where the other angle remains fixed at $116°$. This symmetry breaking is necessary to reach the minimum conical intersection seam that is located between CNNC = $80°$ to $110°$ and CNN = $133°$ and $147°$.

Potential energy surfaces to represent $\hat{V}$ in Eq. 6 were calculated in Ref.[22] on the multistate Restricted Active Space Self Consistent Field (RASSCF) and the Second-Order Perturbation Theory Restricted Active Space (RASPT2) levels of theory with the MOLCAS8 program[31] and using the ANO-L-VDZP basis set.[32] An active space of 18 electrons in 16

15

orbitals was employed, including all π and π^* orbitals and the two nitrogen lone pairs.

Using this, the nuclear grid was discretized with 600 grid points in CNNC and 256 in CNN. After impulsive excitation of the vibrational ground state wavefunction to S_1, the Chebychev propagation scheme[33] was used to numerically integrate Eq. 6 with a time step of 0.05 fs. Impulsive excitation by 100 % is an approximation and usually not achieved in experiment. In case of fractional excitation, a constant background of elastic ground state scattering from the *cis* geometry will be present in the signal, which qualitatively does not influence the structure of the nuclear and electronic scattering terms. The kinetic energy operator $\hat{T}_q$ in Eq. (6) is set up according to the G-Matrix formalism[34] in $M = 2$ reactive coordinates r and s as described in Refs.[35,36]

$$\hat{T}_q \simeq -\frac{\hbar^2}{2m} \sum_{r=1}^{M} \sum_{s=1}^{M} \frac{\partial}{\partial q_r} \left[G_{rs} \frac{\partial}{\partial q_s} \right] \tag{7}$$

with the G-Matrix computed via its inverse elements

$$\left(G^{-1} \right)_{rs} = \sum_{i=1}^{3N} m_i \frac{\partial x_i}{\partial q_r} \frac{\partial x_i}{\partial q_s} \quad . \tag{8}$$

In the S_1 state, periodic boundary conditions are employed along the CNNC torsion. A Butterworth filter[37] was used to absorb the nuclear wavepacket at the borders in the CNN direction, a process that acts as a loss channel and that is not further captured by our Hamiltonian. In S_0 the filter was also employed at $0°$ and $360°$ of torsion. This absorbs the parts of the wavepacket that have reached the product minimum.

Electronic and Nuclear Densities

The state and transition densities $\sigma_{ij}(q, R)$ were evaluated in $2°$ increments in CNNC between $0°$ and $360°$ torsion and CNN bending between $80°$ and $180°$ (a total of 9180 grid points). They were evaluated from the state specific charge density matrices P_{rs}^{ij} according

to

$$\sigma_{E,ij}(\mathbf{q}, \mathbf{R}) = \int dr e^{-i\mathbf{q}\cdot\mathbf{r}} \sum_{rs} P_{rs}^{ij}(\mathbf{R})\phi_r^*(\mathbf{r}, \mathbf{R})\phi_r(\mathbf{r}, \mathbf{R}) \quad , \tag{9}$$

using the basis set of atomic orbitals $\phi_r(\mathbf{r})$. There are a total of 246 $\phi_r(\mathbf{r})$ orbitals for azobenzene in the ANO-L-VDZP basis (14 for each Nitrogen and Carbon and 5 for each Hydrogen). All 96 electrons of azobenzene contribute to the diagonal state densities σ_{ii}, while the transition density consists of one electron located in the nitrogen lone pairs (see Fig. 1(b)).

The nuclear charge density was calculated as

$$\sigma_{N,ij}(\boldsymbol{q}) = \delta_{ij} \int dr e^{-i\mathbf{q}\cdot\mathbf{r}} \int d\boldsymbol{R}\chi_i^*(\boldsymbol{R})\chi_j(\boldsymbol{R}) \sum_a eZ_a \,\delta(\boldsymbol{r} - \boldsymbol{R}_a(\boldsymbol{R})) \tag{10}$$

where $\boldsymbol{R}_a^p(\boldsymbol{R})$ is a function that return the coordinates of the atom a in real space at a given reduced coordinate $\boldsymbol{R}$ and $\chi_i(\boldsymbol{R})$ is the nuclear wavepacket of the state i PES.

Our simulations account for symmetric torsion, i.e. CNNC angles between $+$ and $-180°$. This corresponds to mirroring the azobenzene along the molecular plane and results in the complex real–space densities displayed Fig.3, as both positive and negative torsion values contribute equally.

Acknowledgement

Author contributions

The manuscript was written through contributions of all authors. All authors have given approval to the final version of the manuscript.

References

(1) Zewail, A. H. 4D ultrafast electron diffraction, crystallography, and microscopy. *Annu. Rev. Phys. Chem.* **2006**, *57*, 65–103.

(2) Miller, R. D. Mapping atomic motions with ultrabright electrons: The chemists' Gedanken experiment enters the lab frame. *Annual review of physical chemistry* **2014**, *65*, 583–604.

(3) Sciaini, G.; Miller, R. D. Femtosecond electron diffraction: heralding the era of atomically resolved dynamics. *Reports on Progress in Physics* **2011**, *74*, 096101.

(4) Siwick, B. J.; Dwyer, J. R.; Jordan, R. E.; Miller, R. D. Ultrafast electron optics: Propagation dynamics of femtosecond electron packets. *Journal of Applied Physics* **2002**, *92*, 1643–1648.

(5) Ischenko, A. A.; Weber, P. M.; Miller, R. D. Capturing chemistry in action with electrons: realization of atomically resolved reaction dynamics. *Chemical reviews* **2017**, *117*, 11066–11124.

(6) Kim, H. W.; Vinokurov, N. A.; Baek, I. H.; Oang, K. Y.; Kim, M. H.; Kim, Y. C.;

Jang, K.-H.; Lee, K.; Park, S. H.; Park, S., et al. Towards jitter-free ultrafast electron diffraction technology. *Nature photonics* **2020**, *14*, 245–249.

(7) Chatelain, R. P.; Morrison, V. R.; Klarenaar, B. L.; Siwick, B. J. Coherent and incoherent electron-phonon coupling in graphite observed with radio-frequency compressed ultrafast electron diffraction. *Physical review letters* **2014**, *113*, 235502.

(8) Yang, J.; Zhu, X.; Wolf, T. J.; Li, Z.; Nunes, J. P. F.; Coffee, R.; Cryan, J. P.; Gühr, M.; Hegazy, K.; Heinz, T. F., et al. Imaging CF3I conical intersection and photodissociation dynamics with ultrafast electron diffraction. *Science* **2018**, *361*, 64–67.

(9) Wolf, T. J.; Sanchez, D.; Yang, J.; Parrish, R.; Nunes, J.; Centurion, M.; Coffee, R.; Cryan, J.; Gühr, M.; Hegazy, K., et al. The photochemical ring-opening of 1, 3-cyclohexadiene imaged by ultrafast electron diffraction. *Nature chemistry* **2019**, *11*, 504–509.

(10) Yang, J.; Zhu, X.; Nunes, J. P. F.; Jimmy, K. Y.; Parrish, R. M.; Wolf, T. J.; Centurion, M.; Gühr, M.; Li, R.; Liu, Y., et al. Simultaneous observation of nuclear and electronic dynamics by ultrafast electron diffraction. *Science* **2020**, *368*, 885–889.

(11) Parrish, R. M.; Martínez, T. J. Ab Initio Computation of Rotationally-Averaged Pump–Probe X-ray and Electron Diffraction Signals. *Journal of chemical theory and computation* **2019**, *15*, 1523–1537.

(12) Srinivasan, R.; Lobastov, V. A.; Ruan, C.-Y.; Zewail, A. H. Ultrafast electron diffraction (UED) a new development for the 4D determination of transient molecular structures. *Helvetica chimica acta* **2003**, *86*, 1761–1799.

(13) Keefer, D.; Aleotti, F.; Rouxel, J. R.; Segatta, F.; Gu, B.; Nenov, A.; Garavelli, M.; Mukamel, S. Imaging conical intersection dynamics during azobenzene photoisomerization by ultrafast X-ray diffraction. *Proceedings of the National Academy of Sciences* **2021**, *118*.

(14) Rouxel, J. R.; Keefer, D.; Mukamel, S. Signatures of electronic and nuclear coherences in ultrafast molecular x-ray and electron diffraction. *Structural Dynamics* **2021**, *8*, 014101.

(15) Bennett, K.; Kowalewski, M.; Rouxel, J. R.; Mukamel, S. Monitoring molecular nonadiabatic dynamics with femtosecond X-ray diffraction. *Proceedings of the National Academy of Sciences* **2018**, *115*, 6538–6547.

(16) Rouxel, J. R.; Kowalewski, M.; Bennett, K.; Mukamel, S. X-ray sum frequency diffraction for direct imaging of ultrafast electron dynamics. *Physical review letters* **2018**, *120*, 243902.

(17) Kowalewski, M.; Bennett, K.; Mukamel, S. Monitoring nonadiabatic avoided crossing dynamics in molecules by ultrafast X-ray diffraction. *Structural Dynamics* **2017**, *4*, 054101.

(18) Goulet-Hanssens, A.; Eisenreich, F.; Hecht, S. Enlightening materials with photoswitches. *Advanced Materials* **2020**, *32*, 1905966.

(19) Kienzler, M. A.; Reiner, A.; Trautman, E.; Yoo, S.; Trauner, D.; Isacoff, E. Y. A red-shifted, fast-relaxing azobenzene photoswitch for visible light control of an ionotropic glutamate receptor. *Journal of the American Chemical Society* **2013**, *135*, 17683–17686.

(20) Nägele, T.; Hoche, R.; Zinth, W.; Wachtveitl, J. Femtosecond photoisomerization of cis-azobenzene. *Chemical Physics Letters* **1997**, *272*, 489–495.

(21) Fujino, T.; Arzhantsev, S. Y.; Tahara, T. Femtosecond/Picosecond Time-Resolved Spectroscopy of trans-Azobenzene: Isomerization Mechanism Following S_2 $(\pi\pi^*)\leftarrow$ S_0 Photoexcitation. *Bulletin of the Chemical Society of Japan* **2002**, *75*, 1031–1040.

(22) Aleotti, F.; Soprani, L.; Nenov, A.; Berardi, R.; Arcioni, A.; Zannoni, C.; Garavelli, M. Multidimensional Potential Energy Surfaces Resolved at the RASPT2 Level for Accurate Photoinduced Isomerization Dynamics of Azobenzene. *Journal of Chemical Theory and Computation* **2019**, *15*, 6813–6823.

(23) Quick, M.; Dobryakov, A.; Gerecke, M.; Richter, C.; Berndt, F.; Ioffe, I.; Granovsky, A.; Mahrwald, R.; Ernsting, N.; Kovalenko, S. Photoisomerization dynamics and pathways of trans-and cis-azobenzene in solution from broadband femtosecond spectroscopies and calculations. *The Journal of Physical Chemistry B* **2014**, *118*, 8756–8771.

(24) Aquilante, F.; Autschbach, J.; Carlson, R. K.; Chibotaru, L. F.; Delcey, M. G.; De Vico, L.; Fdez. Galván, I.; Ferré, N.; Frutos, L. M.; Gagliardi, L., et al. Molcas 8: New capabilities for multiconfigurational quantum chemical calculations across the periodic table. 2016.

(25) Kovacs, G. N.; Colletier, J.-P.; Grünbein, M. L.; Yang, Y.; Stensitzki, T.; Batyuk, A.; Carbajo, S.; Doak, R. B.; Ehrenberg, D.; Foucar, L., et al. Three-dimensional view of ultrafast dynamics in photoexcited bacteriorhodopsin. *Nature communications* **2019**, *10*, 1–17.

(26) Yong, H.; Zotev, N.; Ruddock, J. M.; Stankus, B.; Simmermacher, M.; Carrascosa, A. M.; Du, W.; Goff, N.; Chang, Y.; Bellshaw, D., et al. Observation of the molecular response to light upon photoexcitation. *Nature communications* **2020**, *11*, 1–6.

(27) Ma, L.; Yong, H.; Geiser, J. D.; Moreno Carrascosa, A.; Goff, N.; Weber, P. M. Ultrafast x-ray and electron scattering of free molecules: A comparative evaluation. *Structural Dynamics* **2020**, *7*, 034102.

(28) Zheng, J.-C.; Zhu, Y.; Wu, L.; Davenport, J. W. On the sensitivity of electron and X-

ray scattering factors to valence charge distributions. *Journal of applied crystallography* **2005**, *38*, 648–656.

(29) Liu, Y.; Horton, S. L.; Yang, J.; Nunes, J. P. F.; Shen, X.; Wolf, T. J.; Forbes, R.; Cheng, C.; Moore, B.; Centurion, M., et al. Spectroscopic and structural probing of excited-state molecular dynamics with time-resolved photoelectron spectroscopy and ultrafast electron diffraction. *Physical Review X* **2020**, *10*, 021016.

(30) de Kock, M.; Azim, S.; Kassier, G.; Miller, R. Determining the radial distribution function of water using electron scattering: A key to solution phase chemistry. *The Journal of Chemical Physics* **2020**, *153*, 194504.

(31) Aquilante, F.; Autschbach, J.; Carlson, R. K.; Chibotaru, L. F.; Delcey, M. G.; De Vico, L.; Fdez. Galván, I.; Ferré, N.; Frutos, L. M.; Gagliardi, L.; Garavelli, M.; Giussani, A.; Hoyer, C. E.; Li Manni, G.; Lischka, H.; Ma, D.; Malmqvist, P. Å.; Müller, T.; Nenov, A.; Olivucci, M.; Pedersen, T. B.; Peng, D.; Plasser, F.; Pritchard, B.; Reiher, M.; Rivalta, I.; Schapiro, I.; Segarra-Martí, J.; Stenrup, M.; Truhlar, D. G.; Ungur, L.; Valentini, A.; Vancoillie, S.; Veryazov, V.; Vysotskiy, V. P.; Weingart, O.; Zapata, F.; Lindh, R. Molcas8: New capabilities for multiconfigurational quantum chemical calculations across the periodic table. *Journal of Computational Chemistry* **2016**, *37*, 506–541.

(32) Widmark, P.-O.; Malmqvist, P.-Å.; Roos, B. O. Density matrix averaged atomic natural orbital (ANO) basis sets for correlated molecular wave functions. *Theoretica chimica acta* **1990**, *77*, 291–306.

(33) Tal-Ezer, H.; Kosloff, R. An accurate and efficient scheme for propagating the time dependent Schrödinger equation. *The Journal of Chemical Physics* **1984**, *81*, 3967–3971.

(34) Berens, P. H.; Wilson, K. R. Molecular dynamics and spectra. I. Diatomic rotation and vibration. *The Journal of Chemical Physics* **1981**, *74*, 4872–4882.

(35) Thallmair, S.; Roos, M. K.; de Vivie-Riedle, R. Design of specially adapted reactive coordinates to economically compute potential and kinetic energy operators including geometry relaxation. *The Journal of Chemical Physics* **2016**, *144*, 234104.

(36) Reiter, S.; Keefer, D.; Vivie-Riedle, R. *Quantum Chemistry and Dynamics of Excited States*; Wiley, 2020; pp 355–381.

(37) Stephen Butterworth, On the Theory of Filter Amplifiers. *Experimental Wireless and the Wireless Engineer* **1930**, *7*, 536–541.